Modulation of Thiol-Ene Coupling by the Molecular Environment of Polymer Backbones for Hydrogel Formation and Cell Encapsulation

*Burcu Colak[1,2#], Linke Wu[1,2#], Edward J. Cozens[1,2] and Julien E. Gautrot[1,2]**

[1] Institute of Bioengineering and [2] School of Engineering and Materials Science, Queen Mary, University of London, Mile End Road, London, E1 4NS, UK.

* To whom correspondence should be addressed E-mail: j.gautrot@qmul.ac.uk.

[#] These authors contribute equally to this work.

Abstract

Thiol-ene radical coupling is increasingly used for the biofunctionalisation of biomaterials and the formation of 3D hydrogels enabling cell encapsulation. Indeed, thiol-ene chemistry presents interesting features that are particularly attractive for platforms requiring specific reactions of peptides or proteins, in particular *in situ*, during cell culture or encapsulation: thiol-ene coupling occurs specifically between a thiol and a non-activated alkene (unlike Michael addition); it is relatively tolerant to the presence of oxygen; it can be triggered by light. Despite such interest, little is known about the factors impacting polymer thiol-ene chemistry *in situ*. Here we explore some of the molecular parameters controlling photo-initiated thiol-ene coupling (with UV and visible light irradiation), with a series of alkene-functionalised polymer backbones. ^{1}H NMR spectroscopy is used to quantify the efficiency of couplings, whereas photo-rheology allows correlation to gelation and mechanical properties of the resulting materials. We identify the impact of weak electrolytes in regulating coupling efficiency, presumably via thiol deprotonation and regulation of local diffusion. The conformation of associated polymer chains, regulated by the pH, is also proposed to play an important role in the modulation of both thiol-ene coupling and crosslinking efficiencies. Ultimately, suitable conditions for cell encapsulations are identified for a range of polymer backbones and their impact on cytocompatibility is investigated for cell encapsulation and tissue engineering applications. Overall our work demonstrates the importance of polymer backbone design to regulate thiol-ene coupling and *in situ* hydrogel formation.

Keywords

Hydrogel; Thiol-ene; Norbornene; Photo-initiation; Cell encapsulation; Rheology.

Introduction

Thiol-ene radical coupling is now widely used for the development of biomaterials, and in particular for hydrogel design, from scaffolds for 3D cell culture and tissue engineering[1, 2], to controlled release platforms[3, 4] and for the functionalisation of biointerfaces[5, 6] and biosensors[7, 8]. The simplicity with which thiol residues can be introduced in peptide sequences and on polymer backbones has enabled the integration of a wide range of polymer backbones including non-degradable poly(ethylene glycol)-based star polymers[9, 10] and glycosaminoglycans such as hyaluronic acid[11] and chondroitin sulfate[12], to degradable backbones such as gelatin[13]. This flexibility enables the design of multi-functional and responsive matrices, for example allowing the control of mechanical properties, matrix density, charge, cell adhesion or cell-mediated degradability[14-16]. In addition, the cytocompatibility of this coupling, even with UV initiated systems[17], enables the temporal control of mechanical properties[15], cell adhesion[18] and patterning of biomaterials and hydrogels[14, 19].

Although parameters controlling the kinetics and reactivity of alkenes with thiol molecules have been explored extensively, in particular in the context of organic synthesis and hydrophobic resin curing[20-23], the impact of environmental molecular factors on thiol-ene radical chemistry in aqueous media should be studied more extensively. Activated alkenes such as acrylates and methacrylates support radical thiol-ene mechanisms, however these can also result in competing chain growth polymerisations. In contrast, strained norbornene residues are particularly active with respect to thiol-ene propagation and chain transfer steps[21, 23], followed by vinyl ethers and vinyl silazanes. The impact of thiol chemistry has received comparatively less attention, however it has emerged as an important factor regulating thiol-ene radical efficiency[24], primarily through the modulation of the pKa of corresponding thiolates and transfer of radical to moieties, for example present in natural

amino acids. Therefore, such considerations may have a direct impact on the design of bioactive peptide sequences for coupling to biomaterials via thiol-ene coupling or Michael additions. In addition, although a restricted number of photoinitiators have been proposed for UV-light activation (i.e. mainly Irgacure 2959 and lithium acylphosphinate), initiators suitable for visible light activation have also been proposed[25-28]. Although these initiators, including Eosin Y, have the advantage of avoiding the use of UV light and to be very water soluble and cytocompatible, their efficiency for the promotion of radical thiol-ene coupling has not been extensively examined. However, their chemical structure predicts a very strong impact of the molecular environment and pH on their photo-active properties.

In turn, some of the parameters regulating the mechanical properties of radical thiol-ene based hydrogels have been explored. As for other hydrogel design, the concentration of polymer and monomer solutions used during crosslinking has a criticial impact on the macroscopic mechanical properties of thiol-ene hydrogels, with moduli ranging from the 0.1-100 kPa[1, 29-31]. In addition, the degree of functionalisation (either of thiols or alkene residues)[32] and the molecular weight of the polymer backbones also regulate mechanical properties of these hydrogels, as altering the molar mass between crosslinks and regulating local crosslinking densities. In this respect, thiol-ene based networks display better control of local heterogeneity than their counterparts formed via chain growth polymerisation of acrylates and acrylamides (as in polyacrylamide and poly(oligoethylene glycol acrylate))[33], at least prior to swelling, although loop defects are still expected to contribute to delay gelation and alter mechanical behaviours. Finally, the ratio of thiol and alkene residues has been shown to play an essential role in the control of thiol-ene hydrogel mechanics and gelation kinetics[14, 27, 34, 35]. Typically, stoechiometric alkene:thiol ratios typically lead to fastest gelation and highest shear moduli. However, it is often necessary to retain a significant fraction of free alkenes (or thiols, depending on the system) for functionalisation with mono-functional bioactive molecules such as cell adhesive peptides or growth factors.

Therefore, the study of off-stoehiometric hydrogels has important practical applications in the field of tissue engineering.

Comparatively, the impact of macromolecular structure on thiol-ene radical coupling reactivity and how, in turn, this regulates crosslinking and, ultimately, mechanical properties should be further studied. For example, the presence of acidic and basic residues that may alter the charge density along polymer backbones, the local concentration of thiols, the local molecular diffusion and chain conformation, has received little attention with respect to its impact on thiol-ene coupling efficiency and mechanical properties. In this study, a range of alkene-functionalised polymer backbones has been synthesised, displaying polycationic, polyanionic and neutral hydrophilic structures. The impact of such architectures, combined to the pH of the medium, on thiol-ene coupling efficiency is quantified by NMR. In the case of norbornene derivatives, comparisons are made between UV- and visible-light initiated systems. In turn, the impact of this molecular environment on hydrogel mechanics is explored by photo-rheology (Figure 1) and compared to other factors regulating mechanical properties, such as polymer concentration. Finally, we investigate the use of these hydrogels for the encapsulation of endothelial cells and fibroblasts.

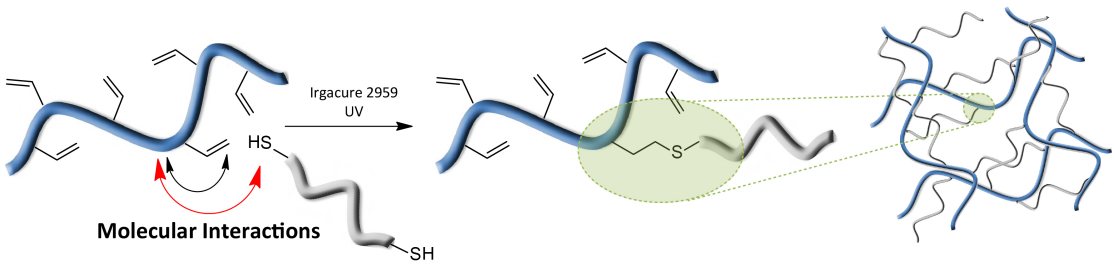

Figure 1. Schematic representation of thiol-ene radical reaction and hydrogel formation based alkene-functionalised polymer backbones and dithiol terminated crosslinkers. The black and red arrows indicate local interactions between the alkene and thiol residues with the molecular structure of the polymer backbone, affecting the efficiency of the thiol-ene coupling.

Experimental section

Materials. Methanol (99.9%), ethanol (99.5%), eosin Y (99 %), Triethanolamine (TEOA, 99%, hydrochloric acid), 1-ethyl-3-(3-dimethylaminopropyl)carbodiimide hydrochloride (EDC), *N*-hydroxysuccinimide (NHS), 3-(trimethoxysilyl)propyl methacrylate (98%), *N*-acetyl *L*-cysteine (99%), allylamine (98%), PBS tablets, Dulbecco's PBS, 2-hydroxy-4'-(2-hydroxyethoxy)-2-methylpropiophenone (IRG2959, 98%), poly(ethylene glycol) dithiol (PEGDT, M_n 1000), triethylamine (99%), 4-pentenoyl chloride (98%), 5-bromo-1-pentene (95%), 2-(dimethylamino)ethyl methacrylate (containing 700-1000 ppm monomethyl ether hydroquinone as inhibitor, 98%), ethyl α-bromoisobutyrate (98%), ethanol (99.8%), 2,2'-bipyridine (>99%), copper (I) chloride (>99.995% trace metals basis), poly(methyl vinyl ether *alt*-maleic anhydride) (M_w ~216 kg/mol average M_n ~80 kg/mol), 2-chloroethylamine hydrochloride (99%), 2-ethyl-2-oxzoline (99%), methyl p-toluenesulfonate (97%), sodium carboxymethyl cellulose (M_w 90 and 250 kg/mol, degree of substitution 0.7), allyl bromide (97%), anhydrous dimethylsulfoxide (>99.9), sodium hydroxide pellets, poly(acrylic acid) (M_v ~450 kg/mol), deuterium oxide (99.9% atom% D), deuterium chloride solution (37 wt% in deuterium oxide, 99% atom% D), sodium deuteroxide (40% in deuterium oxide 99 atom% D), hydrochloric acid (37%), anhydrous magnesium sulphate (99.5%), sodium bicarbonate (99.7%), sodium chloride (99.5%), sodium hydroxide (97%), dichloromethane (99.5%), anhydrous acetonitrile (99.8%), anhydrous dichloromethane (99.8%), anhydrous dimethylformamide (99.8%), methanol (HPLC 99.9%), tetrahydrofuran (99.9%), diethyl ether (99%), , acetonitrile (HPLC 99.9%), heptane (HPLC 99%), dimethylformamide (pharmaceutical secondary standard) and silica gel were obtained from Sigma Aldrich. Chloroform (AnalaR 0.6% of ethanol) and acetone (GPR) was purchased from VWR. Potassium permanganate (98%) was purchased from Alfa Aesar. Chloroform-D (99.8%)

was purchased from Cambridge Isotope Laboratories Inc. Sodium hyaluronic acid (HA, 200 kDa) was purchased from Lifecore ltd. 5-norbornene-2-ethylamine was ordered from Tokyo Chemical Industry Co. Ltd.

Instrumentation. ^{1}H NMR spectroscopy was carried out using a Bruker AV 400 and AVIII 400. Details of assignment of peaks can be found in the Supplementary Information. ATR-FTIR were produced using a Bruker Tensor 27 spectrometer equipped with a MCT detector. Results were acquired at a resolution of 16 cm^{-1} and a total of 128 scans per run in the region of 600-4000 cm^{-1}. A Leica DMI4000B epifluorescent microscope fitted with a HCX PL FLUOTAR 10x/0.3 PJ1 objective and a Leica DFC300 FX CCD camera was used to image cells in 3D hydrogels. Rheological measurements were performed using a DHR-3 rheometer from TA Instruments fitted with a UV accessory and a 20 mm upper parallel plate. The UV curable gels were sandwiched between two coverslips glued to the plates of the rheometer at a fixed gap of 250 μm. Coverslips were functionalised with a monolayer of methacrylate as previously reported[36]: glass coverslips (20 mm) were plasma oxidised for 10 min and incubated in a solution of anhydrous toluene (30 mL) with 3-(trimethoxysilyl)propyl methacrylate (30 μL) and triethylamine (50 μL) for 24 h. The slides were washed with deionised water followed by ethanol and dried under a stream of nitrogen. The glass slides were glued to the quartz bottom plate and top geometry before rheology measurements. Oscillations were set to controlled strain mode at 1 % strain. For *in situ* monitoring of the progression of gelation, a time sweep was performed: 30 s of equilibrium without UV exposure, UV irradiation for 2 min and the UV light was turned off for the remaining part of the experiment. Frequency sweep and amplitude sweep measurements were carried out after UV curing. A Thorlabs fiber light source (400-1300 nm) was used for visible light photo rheology and the light intensity was adjusted to 50 mW/cm^2.

TGA measurements were performed using a TGA Q500 from TA instruments, 25-1000 ºC ramp, 3 ºC/min. TGA traces were analysed to calculate the percentage of water and swelling of the gels. The percentage of water in gels (*W%*) was calculated from the percentage of polymer in the gel (*P*) obtained from the TGA traces: $W\% = 100 - P$ (equation 1). The degree of swelling of gels (Ws) was calculated from the percentage of water in the gel before (*Wi*) and after (*Wf*) swelling in PBS (or water, depending on the conditions): $Ws\ (\%) = (Wf - Wi)/Wi$ (equation 2). GPC analysis was performed using an Agilent 1260 Infinity system equipped with a refractive index and variable wavelength detector, 2 PLgel 5 µm mixed-C column (300 x 7.5 mm), a PLgel 5 mm guard column (50 x 7.5 mm) operated in DMF with NH_4BF_4 (5 mM). The instrument was calibrated with poly(methyl methacrylate) standards (5.5 to 46.9 kg/mol). All samples were filtered through 0.2 µm nylon 66 before analysis.

Statistical analysis. All data were analysed by Tukey's test and significance was determined by * $p < 0.05$, ** $p < 0.01$: *** $p < 0.001$. A full summary of statistical analysis is shown in Tables S1-4.

Synthesis of polymers[37]*. Synthesis and funtionalisation of alkene functional poly(dimethylamino ethyl methacrylate) (**P1**).* The synthesis of PDMAEMA was modified from another protocol (Scheme S1)[38]. A solution of ethanol:deionised water (1:4) was prepared and degassed for 30 min. 2-(dimethylamino) ethyl methacrylate (0.0954 mol) was weighed into a flask containing ethyl α-bromoisobutyrate (0.00037 mol), dissolved in ethanol-water 1:4 (7.5 mL) and degassed for 30 min. Into a second flask, 2,2'-bipyridine (0. 19 mmol) was weighed dissolved in ethanol-water 4:1 (7.5 mL) and degassed for 30 min. To the 2,2'-bipyridine solution was added copper (I) chloride (0.19 mmol), the brown solution was sonicated for 10 minutes. The catalyst solution was transferred to the monomer solution and the reaction was stirred under inert atmosphere for 5 h at 50 ºC. The ethanol was

evaporated prior to freeze-drying of the remaining solution. The obtained solid was dissolved in tetrahydrofuran and added to silica gel (20 g), agitated for 1 h, filtered and concentrated using a rotary evaporator, then precipitated in heptane, filtered and dried under reduced pressure. PDMAEMA characterisation: GPC, M_n 67.9 kg/mol, $Đ_M$ 1.6. ^{1}H NMR, (400 MHz; D_2O) δ 0.75-1.2 (3H, m), 1.7-2.0 (2H, m), 2.3 (6H, s), 2.6-2.8 (2H, m) and 4.1 (2H, m) (Figure S1a). FTIR, *v/cm^{-1}* 2900 (w, C-H), 1720 (s, C=O), 1261 (m, C-N) and 1100 (s, C-O).

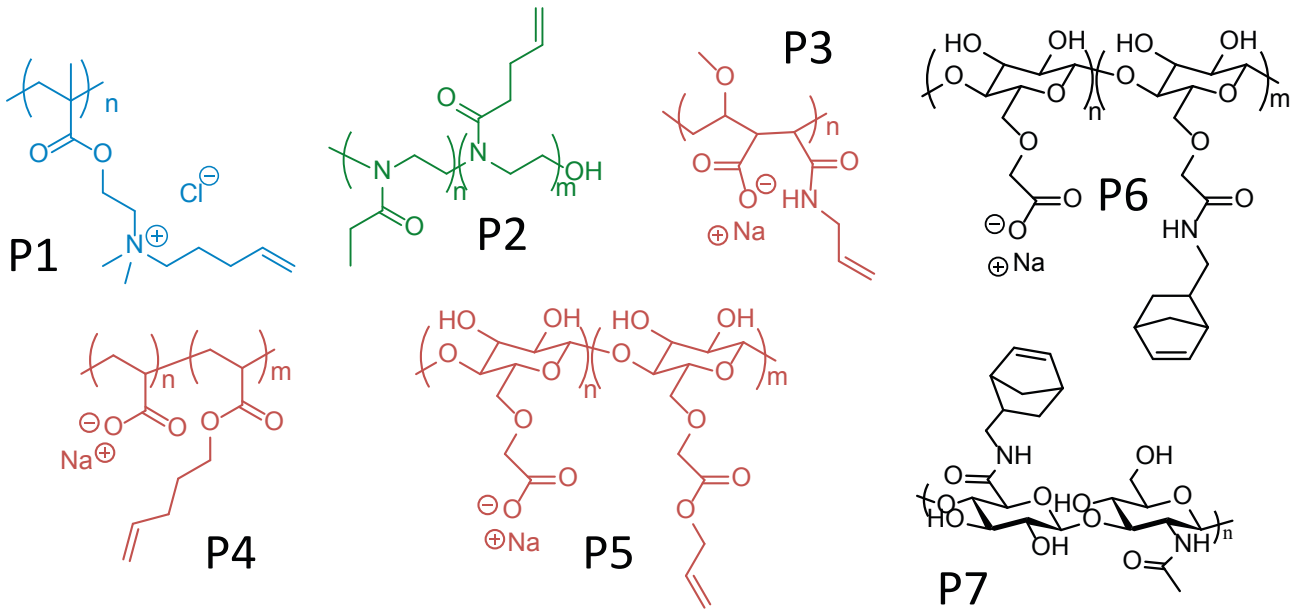

Scheme 1. Chemical structure of the different alkene-functionalised polymers studied.

PDMAEMA (1 eq., 1 g, 0.0064 mol) was then dissolved in dimethylformamide (10 mL), and 5-bromo-1-pentene (2.5 eq., 0.015 mol) was added before the reaction mixture was stirred overnight at 70 ºC. The resulting polymer was precipitated in diethyl ether and the remaining solid was dissolved in methanol and precipitated in diethyl ether. The recovered polymer was precipitated from methanol twice more. The polymer (**P1**) was recovered and dried under reduced pressure. ^{1}H NMR, (400 MHz; D_2O) δ 0.85-1.4 (3H, m), 1.9-2.1 (2H, m), 2.1-2.3 (4H, m), 3.3 (6H, s), 3.4-3.5 (2H, m), 3.7-4.0 (2H, m), 4.3-4.6 (2H, m) 5.0-5.2 (2H, m) and 5.8-6.0 (1H, m) (Figure S1b). FTIR, *v/cm^{-1}* ~2900 (w, C-H), 1727 (s, C=O), 1643 (w,

C=C), 1243 (m, C-N) and 1137 (s, C-O) (Figure S2). GPC M_n 67.9 kg/mol, $Đ_M$ 1.60 measured in DMF with NH_4BF_4 (5 mM). The alkene functionalisation level was calculated as 100 %.

Synthesis of 2-butenyl-2-oxazoline. The monomer 2-butenyl-2-oxazoline was synthesised following an adapted protocol reported by Gress *et al* (Scheme S2).[39] 2-chloroethylamine hydrochloride (1.2 eq., 0.092 mol) was transfered to a round bottom flask and purged with inert gas for 30 minutes. Anhydrous dimethylformamide (80 mL) was subsequently added, under inert atmosphere. The flask was placed into an ice bath under inert gas atmosphere and triethylamine (2.5 eq., 0.194 mol) was added, followed by dichloromethane (75 mL) and pentenoyl chloride (1 eq., 0.077 mol). The reaction was stirred in a water bath for 24 h under inert atmosphere. A brown solution and cream precipitate formed. The flask content was added into a separation funnel with dichloromethane (200 mL). With the addition of dichloromethane, the precipitate dissolved. The organic solution was extracted from hydrochloric acid (1M, 500 mL four times), saturated sodium carbonate (500 mL twice), then from brine (500 mL, four times). The organic layers were recovered and dried over magnesium sulphate. The organic layer was evaporated to yield a brown oil. ^{1}H NMR, (400 MHz; $CDCl_3$) 2.2-2.35 (4H, m), 3.55 (4H, m), 4.9-5.0 (2H, m) and 5.7-5.9 (1H, m). Crushed potassium hydroxide (1eq., 0.08 mol) was added to an oven-dried round bottom flask and the system was purged with inert gas for 30 min. Dry methanol (40 mL) was added, followed by N-(2-chloroethyl)-4-pentenamide (1eq.). The reaction was heated to 70 ºC for 24 h. The potassium chloride salt that precipitated was filtered and the remaining solution was evaporated. The content was distilled over calcium hydride to yield a clear oil. ^{1}H NMR, (400 MHz; $CDCl_3$) 2.4 (4H, m), 3.8 (2H, t), 4.3 (2H, t), 5.0-5.1 (2H, m) and 5.8-5.9 (1H, m). FTIR, $\tilde{\nu}$/cm^{-1} ~2900 (w, C-H), 1675 (s, C=O), 1174 (w, C-N).

*Synthesis of poly(2-butenyl-2-oxazoline)-co-(2-ethyl-2-oxazoline) (**P2**).*

2-Ethyl-2-oxazoline (distilled over calcium hydride, 80 eq., 0.08), 2-butenyl-2-oxazoline (20 eq.) and anhydrous acetonitrile (20 mL) were added into a microwave flask containing a magnetic stirrer. Methyl *p*-toluenesulfonate (1 eq.) was then added against a flow of nitrogen. The reaction vessel was heated using a microwave reactor, 140 ºC for 30 minutes.[40] The reaction was terminated by addition of a drop of water and precipitated in cold diethyl ether three times. The remaining polymer (**P2**) was recovered and dried under reduced pressure. ^{1}H NMR, (400 MHz; $CDCl_3$) 1.1 (2H, m), 2.1-2.5 (8H, m), 3.4 (2H, m), 5.0 (2H, m) and 5.8 (1H, m) (Figure S3). FTIR, ν/cm^{-1} ~3400 (br, O-H), ~2900 (w, C-H), 1633 (s, C=O), 1180 (w, C-N) (Figure S4). The copolymer composition was calculated as 15% of butenyl side chains. GPC M_n 6.3 kg/mol, $Đ_M$ 1.62 measured in DMF with NH_4BF_4 (5mM).

*Synthesis of allylamine functionalised poly(methyl vinyl ether alt-maleic anhydride) (**P3**).* Allylamine (1 eq., 0.08 mol) was dissolved in acetonitrile (250 mL). Poly(methyl vinyl ether *alt*-maleic anhydride) (1eq.) was dissolved in acetonitrile (200 mL) in a second flask. The poly(methyl vinyl ether *alt*-maleic anhydride) solution was slowly added to the amine solution with vigorous stirring. On addition of poly(methyl vinyl ether *alt*-maleic anhydride) to the allylamine, a white precipitate formed. The mixture was stirred at 70 °C for 24 h and room temperature for 48 h. The acetonitrile was evaporated and dissolved in distilled water. The polymer (**P3**) was precipitated in acidic water and recovered by freeze drying (Scheme S3). ^{1}H NMR, (400 MHz; D_2O) 1.3-2.2 (2H, m), 2.5-3.0 (2H, m), 3.1-3.5 (3H, m), 3.6-3.8 (2H, m), 4.0-4.2 (1H, m), 5.0-5.3 (2H) and 5.6-5.9 (1H, m) (Figure S5). FTIR, ν/cm^{-1} ~3400 (br, O-H), ~2900 (w, C-H), 1556 (s, C=O), 1388 (w, C-N) and 1072 (w, C-O) (Figure S6). The functionalisation ratio was found to be quantitative (100%).

*Synthesis of poly(acrylic acid-co-pentenyl acrylate) (**P4**).* Poly (acrylic acid) (1 eq., 5 g, 0.069 mol) was dissolved in a sodium hydroxide solution (1 mol/L, 52.5 mL). 5-bromo-1-pentene

(0.25 eq., 0.0174 mol) was dissolved in dimethylformamide (10 mL) and the resulting solution was then transferred to the poly (acrylic acid) solution. The mixture was heated to 70 °C overnight. The cooled reaction mixture was precipitated in acetone: diethyl ether (3:1) redissolved in deionised water and precipitated in acetone again. The polymer **P4** was dried under reduced pressure (Scheme S4). ^{1}H NMR, (400 MHz; D_2O) δ 1.5-1.7 (6H, m), 2.1 (1H, m), 4.0 (2H, m), 5.0 (2H, m), and 5.86 (1H, m) (Figure S7). FTIR, *v/cm^{-1}* ~3400 (w. O-H), ~2900 (w, C-H), 1679 (m, C=O) and 1552 (s, C=O) (Figure S8). The functionalisation ratio was calculated as 5.2 %.

*Synthesis of carboxymethyl cellulose allyl ester (**P5**).* Sodium carboxymethyl cellulose (1 eq., 0.0048 mol) was dissolved in distilled water (50 mL) and a solution of allyl bromide (0.76 eq., 0.00366 mol) in dimethylsulfoxide (50 mL) was added to this mixture, and stirred overnight at 70 °C. The resulting product **P5** was purified by two successive precipitation in acetone and dried under reduced pressure (Scheme S5). ^{1}H NMR, (400 MHz; D_2O) δ 3.2-4.6 (18H, m) 5.45 (2H, m) and 6.0 (1H, m) (Figure S9). FTIR, *v/cm^{-1}* ~3300 (m, O-H), ~2900 (w, C-H), 1589 (s, C=O) and 1008 (s, C-O) (Figure S10). The functionalisation ratio was calculated as 13.4%.

*Synthesis of functionalised norbornene-carboxymethyl cellulose (**P6**) and norbornene-functionalised hyaluronic acid (**P7**).* Functionalised CMC-NB (**P6**) was synthesised following a protocol adapted from the literature[41]. In brief, 0.25 g (1.2 mmol of repeat units) of sodium CMC (CMC 90 kDa was used for NMR experiment whereas CMC 250 kDa was used for rheology and gelation studies) were dissolved in 25 mL deionized water. 0.148 g (0.77 mmol) EDC and 89 mg (0.77 mmol) NHS were added to the solution, prior to 0.1 mL (0.8 mmol) of 5-norbornene-2-ethylamine. The solution became cloudy and was left to stir for 18 to 24 h at room temperature. The solution was added dropwise to 250 mL ice-cold acetone containing sodium chloride (0.75 g) and stirred for an hour at room temperature. Acetone

was decanted to yield a white precipitate. The precipitate was dissolved in 22 mL of deionized water and dialyzed for 3 d prior to removing water by lyophilization, affording a white powder of purified CMC-NB **P6**. ^{1}H NMR (400 MHz; D_2O) δ 3.2-4.6 (18H, m) and 5.9-6.4 (2H, m). The functionalisation ratio was calculated as 22.5%**.** HA-NB (**P7**) was synthesized following the same protocol. ^{1}H NMR (400 MHz; D_2O) δ 1.8 (3H, m) 5.9-6.4 (2H, m). The functionalisation ratio was calculated as 19%.

Quantification of thiol-ene coupling efficiency via ^{1}H-NMR. Thiol-ene coupling between the different polymers studied (**P1-P3**, 45 mM with respect to alkenes) and *N*-acetyl *L*-cysteine (45.4 μmol, 45 mM) was quantified by ^{1}H NMR, in deuterated-PBS (1 mL; see Scheme S6 for model reaction with **P2**). A stock solution for Irgacure 2959 was prepared in methanol (0.198 M, 0.0444 g/mL). 5 mol % (12.5 μL; final concentration of 2.25 mM) of photoinitiator were added to the polymer mixture from this stock solution. The pH of the solutions was adjusted using the NaOD or DCl. The samples were irradiated with UV (17 mW/cm^2, 350−500 nm) 300 s (power 5.10 J/cm^2). The UV light source (strictly speaking blue to UV light) used to initiate reactions was an Omnicure series 1500 lamp. An ILT 1400-A radiometer photometer from international light technologies was used to measure the UV light intensity. ^{1}H NMR was analysed (Figure S11 for examples for **P2**) and conversions were calculated via the consumption of the alkene peaks with respect to the formation of the product peaks.

To study coupling with **P4**, a similar protocol was used, with the following changes: *N*-acetyl *L*-cysteine (14 μmol, 14 mM) and alkene-functionalised polymer (**P4**) (0.025 g, 14 μmol, 14 mM) were dissolved in deuterated-PBS. To these thiol−ene solutions were added 1 mol % (final concentration, 140 μM) photoinitiator from the stock solution. The pH values of the solutions were adjusted prior to irradiation with UV light (300 s, 52 mW/cm^2 15.6 J/cm^2). For coupling with **P5**, *N*-acetyl *L*-cysteine (23.6 μmol, 23.5 mM) and the alkene-functionalised

polymer **P5** (0.05 g, 23.5 μmol, 23.5 mM) were dissolved in deuterated-PBS (1 mL). To these thiol−ene solutions was added 4.4 mol % (1 mM final concentration) photoinitiator from stock solution. The pH values of the solutions were adjusted and irradiated with UV as above (300 s, 5.10 J/cm^2). For coupling with **P6**, *N*-acetyl *L*-cysteine (34.5 μmol, 34.5 mM) and the norbornene-functionalised **P6** (0.05 g, 34.5 μmol, 34.5 mM) were dissolved in deuterated-PBS (1 mL, 1:1 thiol:alkene ratio). To the thiol−ene solution was added 5 mol % (1.725 mM) of photoinitiator from a stock solution. The pH value of the solutions was adjusted and the resulting solutions were irradiated with UV as above (300 s, 5.10 J/cm^2).

Hydrogel preparation. To make hydrogels for mechanical characterisation and swelling, solutes were dissolved in PBS: polymer backbones (**P1-P7**), crosslinkers (PEGDT) and IRG 2959 (from a 250 mg/mL solution in in methanol). Crosslinked hydrogels (thiol:ene 0.5:1 for **P1-P4** and 0.64:1 for **P5**) were generated see Tables 1 and 2 for details. For **P5**, **P6** and **P7** gels at different pH, solutions at 10 mg/mL were prepared and the pH of the gel mixture was altered using sodium hydroxide or hydrochloric acid. The gel mixtures were transferred to the rheology geometry (quartz plate), for characterisation of shear properties, and 8 mm cylindrical moulds for TGA and FTIR characteristion. Curing was carried out using an Omnicure series 1500 lamp 320-500 nm light source (17 mW/cm^2, power 2.04 J/cm^2). Samples for TGA and FTIR characterisation were cured for 120 s. Hydrogels cured using visible light (400-1300 nm, 50 mW/cm^2) were irradiated for 150 s in the presence of 0.005% EY (w/v) and 0.1% TEOA (v/v) (see Table 3). Hydrogels were characterised by FTIR-ATR after dehydration (Figure S12), confirming the retention of the expected chemical structure and combination with bands associated with the crosslinker (poly(ethylene glycol) dithiol; C-O stretching vibration at 1050-1100 cm^{-1}).

Table 1. The concentrations of the components used to generate gels from **P1-P3** in molar concentration and mg/mL. Gels were made using thiol:ene 0.5:1 mol ratio, 5 mol% photoinitiator and 120 s UV exposure (17 mW/cm^2). Average modulus (kPa) and average time taken to reach maximum storage modulus (G_t) have been reported (from experiments carried out at pH 7.4).

Gel	Alkene conc^n (mM)	Thiol conc^n (mM)	Thiol:ene ratio	Alkene (mg/mL)	PEGDT (mg/mL)	IRG 2959 (mg/mL)	Modulus (kPa)	G_t (s)
P1$_{S2}$	90	45	0.5:1	18.2	22.5	0.51	No gel	-
P1$_{S3}$	135	67.5	0.5:1	27.3	33.8	0.76	0.480	101
P1$_{S4}$	180	90	0.5:1	36.4	45	1.01	2.35	100
P1$_{S5}$	225	112.5	0.5:1	45.5	56.3	1.27	7.47	97
P2$_{S2}$	90	45	0.5:1	60.7	22.5	0.51	0.429	100
P2$_{S3}$	135	67.5	0.5:1	91.1	33.8	0.76	5.11	63
P2$_{S4}$	180	90	0.5:1	121.5	45	1.01	11.09	62
P2$_{S5}$	225	112.5	0.5:1	151.8	56.3	1.27	16.38	60
P3$_{S2}$	90	45	0.5:1	19.2	22.5	0.51	0.155	118
P3$_{S3}$	135	67.5	0.5:1	28.8	33.8	0.76	1.41	111
P3$_{S4}$	180	90	0.5:1	38.4	45	1.01	5.3	107
P3$_{S5}$	225	112.5	0.5:1	48.0	56.3	1.27	11.08	97
P4$_{S2}$	90	45	0.5:1	154.7	22.5	0.51	3.22	112
P4$_{S3}$	135	67.5	0.5:1	232.0	33.8	0.76	17.75	111
P4$_{S4}$	180	90	0.5:1	309.3	45	1.01	No gel	-
P4$_{S5}$	225	112.5	0.5:1	386.7	56.3	1.27	No gel	-

Table 2 The concentration of the components used to generate gels from **P5-P7** in molar concentration and mg/mL. Gels were generated using 120 s UV exposure exposure (17 mW/cm^2). Average modulus (kPa) and average time taken to reach maximum storage modulus (G_t) are also reported (from experiments carried out at pH 7.4).

Gel	Alkene conc^n (mM)	Thiol conc^n (mM)	Thiol:ene ratio	Alkene (mg/mL)	PEGDT (mg/mL)	IRG 2959 (mg/mL)	Modulus (kPa)	G_t (s)
P5$_5$	2.35	1.5	0.64:1	5	0.65	0.17	0.189	109
P5$_{10}$	4.7	3.0	0.64:1	10	1.3	0.33	0.465	89
P5$_{20}$	9.4	6.0	0.64:1	20	2.6	0.67	1.929	85
P6$_{uv}$	5.2	5.2	1:1	10	2.6	0.064	0.624	41
P7$_{uv}$	4.85	4.85	1:1	10	2.42	0.064	0.706	37

Table 3 The concentration of components used to generate gels from **P6-P7** via visible light mediated photo-initiation, in molar concentrations and mg/mL. Gels were cured for 120 s with visible light exposure (50 mW/cm^2) in the presence of 0.1 v/v% TEOA. Average modulus (kPa) and average time taken to reach maximum storage modulus (Gt) are also reported (from experiments carried out at pH 7.4).

Gel	Alkene conc^n (mM)	Thiol conc^n (mM)	Thiol:ene ratio	Alkene (mg/mL)	PEGDT (mg/mL)	EY (w/v%)	Modulus (kPa)	G_t (s)
P6$_{EY}$	5.17	5.2	1:1	10	2.6	0.005	0.519	69
P7$_{EY}$	4.85	4.85	1:1	10	2.42	0.005	0.255	101

Cell culture in hydrogels. HUVECs (Lonza, C2519A) were routinely grown in EBM-2 supplemented with ECGF. For fibroblast culture, HCA2 dermal fibroblasts were used[42]. Cells were routinely grown in DMEM supplemented with 10% FBS, 1% penicillin streptomycin and 1% glutamine. The medium was changed every 2-3 days and cells were sub-cultured each week using trypsin/versene. Cells were maintained at 37ºC in a humidified atmosphere containing 5% CO_2. Hydrogels for cell culture were generated from corresponding polymer solutions in PBS (refer to Table 4). Solutions in PBS were filtered through a 0.2 µm supor membrane pore for sterilisation. Cells were added (HUVECs passage 2-5, 1 million cells/mL gel; dermal fibroblasts, 0.5 million cells/mL gel) and cured using UV light (120 s, 17 mW/cm^2, power 2.04 J/cm^2). Gels with 3D encapsulated cells were washed with PBS and medium before adding medium and incubation for 24 h. The medium used for HUVECs was EBM-2 and for dermal fibroblasts was DMEM. Live/dead assays were performed on the 3D encapsulated cells at 24 h to study the cell viability. Cells were stained green with calcein (0.5 µL/mL) and red with ethidium homodimer-1 (2 µL/mL) in medium (serum-free) for 20 minutes, washed with medium and incubated 15 minutes before imaging. Epifluorescence images were produced using 10x objective and analysed using Image J. Penicillin streptomycin (5000 U/mL), Calcein was obtained from life technologies. FBS, South American Origin was purchased from Labtech. DMEM and calcein were obtained from life technologies. L-glutamine (200 mM), versene, trypsin (0.25%) phenol red and ethidium homodimer-1.were obtained from Thermo Fisher Scientific. HUVECs medium EBM-2 was purchased from Lonza. Custom peptides GCGGRGDSPG (RGD) and GCRDVPMS↓MRGGDRCG (VPM) (↓ indicates the cleavage site) were purchased from Proteogenix, France.

Table 4 The concentration of the components used to generate **P2** gels in molar concentration and weight percent. Gels were generated using a thiol:ene 0.5:1 ratio (for polymer and crosslinkers), 10 mol% RGD, 0.5 mol% PI and 120 s UV exposure.

Gel VPM:PEGDT	Alkene concn (mM)	Thiol concn (mM)	Thiol-ene ratio	P2 (mg/mL)	PEGDT (mg/mL)	VPM (mg/mL)	RGD (mg/mL)	IRG 2959 (mg/mL)
$P2_{S3}$	135	67.5	0.5:1	91.1	33.8	0	12	0.76
$P2_{S4}$	135	67.5	0.5:1	91.1	33.8	0	12	0.76
$P2_{S5}$	135	67.5	0.5:1	91.1	33.8	0	12	0.76
$P2_{S3}$ 100:0	135	67.5	0.5:1	91.1	0	57.3	12	0.76
$P2_{S3}$ 75:25	135	67.5	0.5:1	91.1	8.5	42.9	12	0.76
$P2_{S3}$ 50:50	135	67.5	0.5:1	91.1	16.9	28.6	12	0.76
$P2_{S4}$ 75:25	180	90	0.5:1	121.5	11.3	57.3	16	1.01
$P2_{S5}$ 75:25	225	112.5	0.5:1	151.8	14.1	71.6	19	1.27

Results and dicussion

Effect of the molecular environment on thiol-ene coupling efficiency. Given the importance of the protonation state of thiols to the formation of thiyl radicals[24, 43], we first investigated the impact of pH on coupling efficiencies to the model thiol acetyl cysteine to a range of alkene-functionalised hydrophilic polymers (with thiol:olefin ratios of 1:1). We selected these polymers based on their neutrality (for the poly(2-alkyl-2-oxazoline) polymer **P2**) and their charge (positively charged as for the quaternized poly(dimethylaminoethyl methacrylate) **P1** and negatively charged for the maleic anhydride copolymer **P3**, the functionalised poly(acrylic acid) **P4** and carboxymethyl cellulose **P5**; see Scheme 1). Polyelectrolytes such as poly(acrylic acid), carboxymethyl cellulose and hyaluronic acid are often used as backbones for the formation of hydrogels via thiol-ene chemistry. By selecting a range of poly(anions) with a range of charge density (**P3-P5**), we aimed to investigate how such electrostatic environment would impact on thiol-ene coupling.

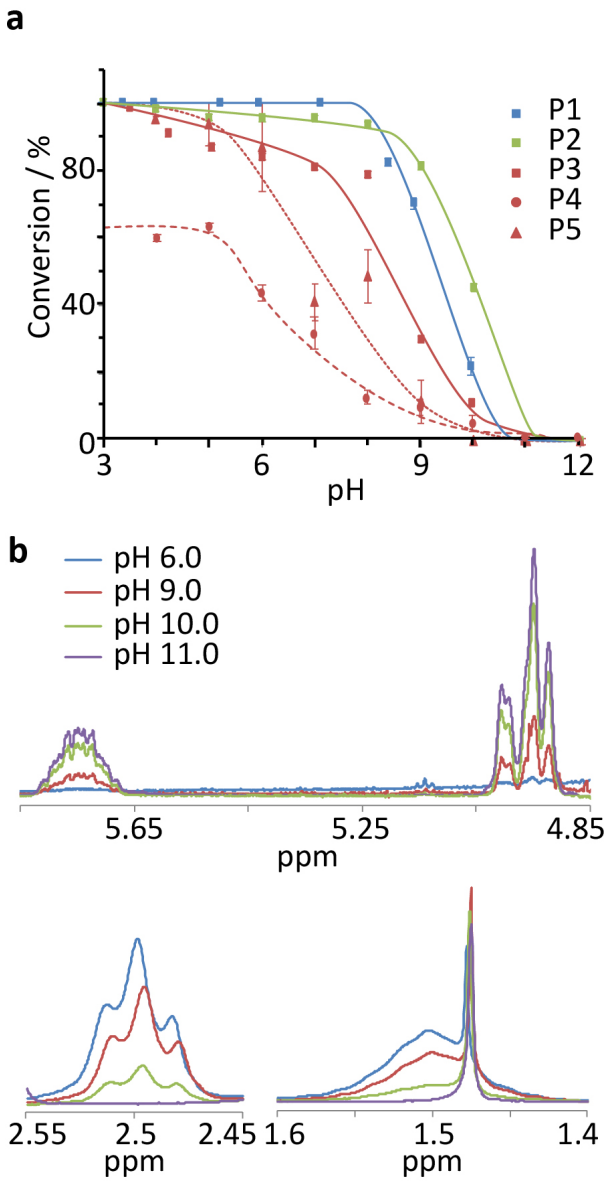

Figure 2. a) Impact of the backbone chemistry and pH of the reaction milieu on thiol-ene conversion with *N*-acetyl *L*-cysteine (thiol:ene 1:1, 45μM, 5 mol% photoinitiator, 300 s UV exposure, 17 mW/cm^2). Lines are only intended as a guide for the eye. b) ^{1}H NMR spectra for the thiol-ene reaction of polymer **P2** with *N*-acetyl *L*-cysteine, focusing on the alkene protons and those associated with the formation of thioether, at different pH.

To mimic the environment typically used for the *in situ* formation of hydrogels for cell encapsulation or tissue engineering, thiol-ene radical coupling was carried out in deuterated phosphate buffer saline and monitored by ^{1}H NMR (Figure 2a and b, Scheme S6 and Figure S11) and initiated by Irgacure 2959. Advancement of these reactions at different pH was quantified via the integration of peaks associated with protons adjacent to the thiol and formed thioeter, compared to those of alkene protons. For **P1** and **P2**, coupling was found

to be efficient (> 95 %) up to pH 7.0, prior to sharp decrease at higher pH, due to the predominance of the thiolate forms of acetyl cysteine in basic conditions (pKa of 9.5[24, 44]). This is consistent with coupling efficiencies previously reported at different pH in PBS for model thiol-ene coupling reactions[24]. For terminal olefins, coupling was found to be efficient at low to neutral pH prior to sharply decreasing, depending on the pKa of the thiol involved. Hence it was identified that terminal cysteines are poorer anchors for radical thiol-ene coupling than acetyl or non-terminal cysteines, due to the reduction of their pKa. Consistent with this report, the polycation **P1** displayed high reaction efficiencies as the olefin is sufficiently distant from the ammonium group to avoid overlap of the single occupied molecular orbital, centered on the carbon radical in the transition state, with the ammonium residue[24].

In contrast, coupling of acetyl cysteine to negatively charged polymers was substantially reduced (Figure 2a). Thiol-ene reaction efficiency was above 80% at pH below 7.0 for **P3** and **P5**, below the coupling observed for **P1** and **P2**. However, the striking reduction in thiol-ene efficiency observed at higher pH (> 8.0-9.0) for **P1** and **P2** occurred at lower pH in the case of **P3** and **P5**. Strikingly, thiol-ene efficiency to the pentenyl-functionalised poly(acrylic acid) **P4** was reduced to 60% at pH 4.0-5.0 and the drop observed at higher pH occurred as early as pH 6.0, with efficiencies below 30% at pH above 7.0. Therefore, an increase in the density of carboxylate groups is clearly associated with a reduction in thiol-ene efficiency. Despite local pH effects, which will result in a significant level of protonation even at neutral pH[45, 46], a high negative potential is expected within polyanionic electrolytes. As a result, this local increase in negative charge density may alter the diffusion of negatively charged small molecules, such as acetyl cysteine, and prevent accessibility to alkene residues.

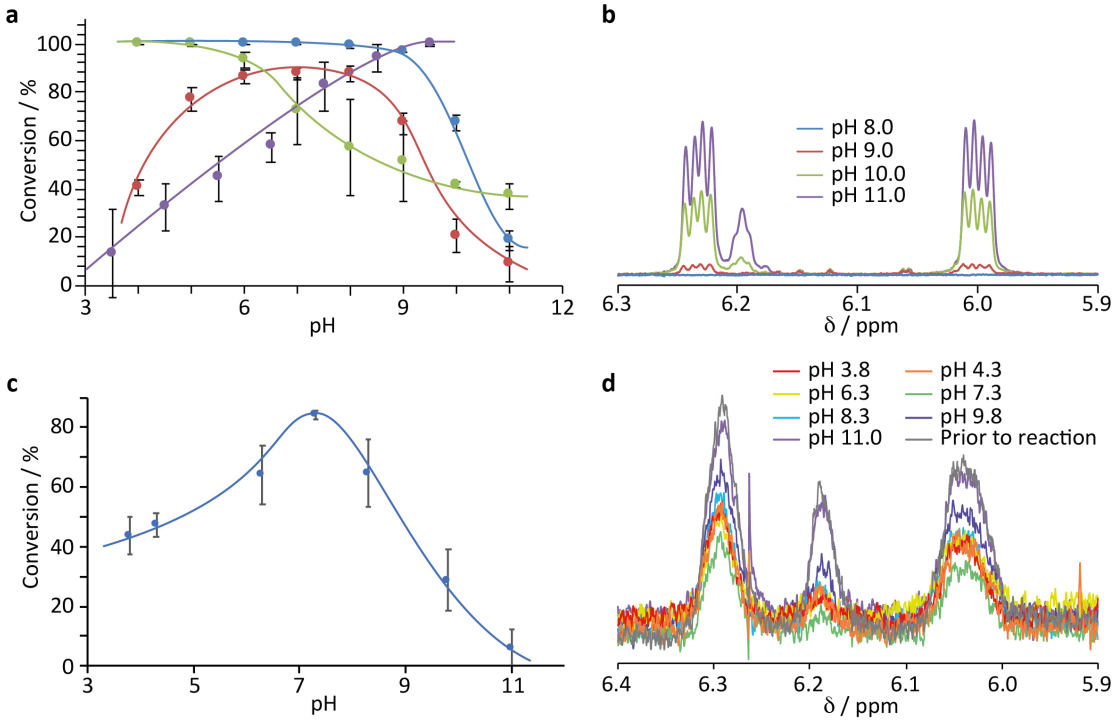

Figure 3. a) Series of alkene reacted with N-acetyl-L-cysteine (Thiol:ene 1:1, 45 µM). With UV irradiation: 5 mol% Irgacure 2959, 300 s exposure at 17 mW/cm^2. Blue, 5-Norbornene-2-carboxylic acid; Green, norbornene derivative **1**. With visible light irradiation: 0.005% (w/v) Eosin Y and 0.1% (/v) TEOA, 300 s exposure at 50 mW/cm^2. Red, 5-Norbornene-2-carboxylic. For Michael addition, PEG acrylate solutions were mixed with N-acetyl-L-cysteine solutions and allowed to react for 5 min prior to NMR characterisation. Purple, PEG acrylate. Lines are only intended as a guide for the eye. b) Examples of ^{1}H NMR spectra (alkene peaks only) for the thiol-norborene reaction (UV initiated) between 5-Norbornene-2-carboxylic acid and N-acetyl-L-cysteine, at different pH. c) Impact of pH on thiol-ene coupling between **P6** (50 mg/mL, 90 kDa) and N-acetyl-L-cysteine (thiol:ene 1:1, 45 µM, 5 mol% photoinitiator, 300 s UV exposure, 17 mW/cm^2). d) Corresponding examples of ^{1}H NMR spectra of alkene (norbornene).

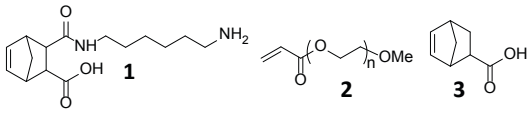

Scheme 2. Chemical structure of the different alkenes used in NMR experiments (see Figure 3).

Impact of the molecular environment on thiol-ene coupling with nobornene derivatives. Norbornene-functionalised polymers have become widely used for the generation of hydrogels via thiol-ene radical coupling due to their high reactivity even in dilute conditions, in the presence of oxygen, and without significant unwanted chain growth radical polymerisation[14, 35, 47, 48]. These compounds can be introduced onto polymer backbones via ester, amide or ether bonds, however the impact of the local molecular environment and the pH of the media has not been systematically investigated in these systems. Hence we first examined the impact of the pH of the medium on thiol-ene radical

coupling to norbornene derivatives (initiated with UV light irradiation and Irgacre 2959; see Figure 3a and b). Similarly to the coupling of acetyl cysteine to non-activated terminal olefins, we observed high reaction effiencies in the case of 5-Norbornene-2-carboxylic acid at low to neutral pH, followed by a marked decrease at higher pH. However, efficiencies above 99% were retained up to pH 9.0, likely due to the higher reactivity of this alkene, therefore enabling coupling even a pH for which significant thiolates are formed. In comparison, Michael addition of acetyl cysteine to a poly(ethylene glycol) acrylate was associated with a linear coupling efficiencies as the pH of the medium increased (Figure 3a), consistent with the importance of thiolates for this reaction. Surprisingly, a carbic anhydride derivative functionalised with hexane-1,6-diamine (compounds **1**, Scheme 2) was found to display reduced efficiencies at lower pH (above pH 6.0). This may be due to a greater steric hindrance and potentially the increased hydrophobicity associated with this compound.

In addition to their high reactivity in thiol-ene coupling initiated by UV-active photoinitiators such as Irgacure 2959 and lithium phenyl-2,4,6-trimethylbenzoylphosphinate, reactive olefin-functionalised polymers have been cured via visible light initiated systems, for example using Eosin Y[25, 28, 30]. However, the impact of pH on this polymerisation system has not been studied. Therefore, we investigated the impact of Eosin Y initiated visible light activated radical coupling of acetyl cysteine to norbornene carboxylic acid (Figure 3a). Similarly to UV-initiated systems, reactivities were high (above 87%) within pH 6.0-8.0, confirming the potential of visible light curing for *in situ* hydrogel formation. Above this pH range, thiolates are again starting to dominate, leading to a reduction in coupling. However, below a pH of 6.0, we also observed a significant decrease in efficiency, presumably due to the protonation of Eosin Y. Hence visible light activated thiol-ene coupling to norbornene residues is expected to be stable within a reasonably wide range of pH, relevant to *in situ* cell encapsulation and loading within degradable hydrogels.

Finally, we investigated the coupling of acetyl cysteine to the norbornene-functionalised carboxymethyl cellulose **P6** (Figure 3c and d). As for other polyanions tested, thiol-ene coupling decreased drastically at elevated pH (8.0 and above), due to thiolate prevalence. Coupling was optimal at pH 7.4, with efficiencies of 84%. At lower pH, a reduction of coupling down to 43% was also observed, in contrast to the radical thiol-ene coupling observed for **P5** and the two low molar mass norbornene derivatives tested (Figure 3a and b). The origin of this behaviour is unclear, but may be due to the more hydrophobic character of norbornene residues compared to pentene side chains, leading to more shielded structures as carboxymethyl cellulose protonates at lower pH and collapses. Overall, our results clearly demonstrate the strong impact that the molecular structure of polymer backbones, coupled to their pH-responsive behaviour and the acid-base properties of thiols and initiator molecules, play in determining radical thiol-ene tethering efficiencies.

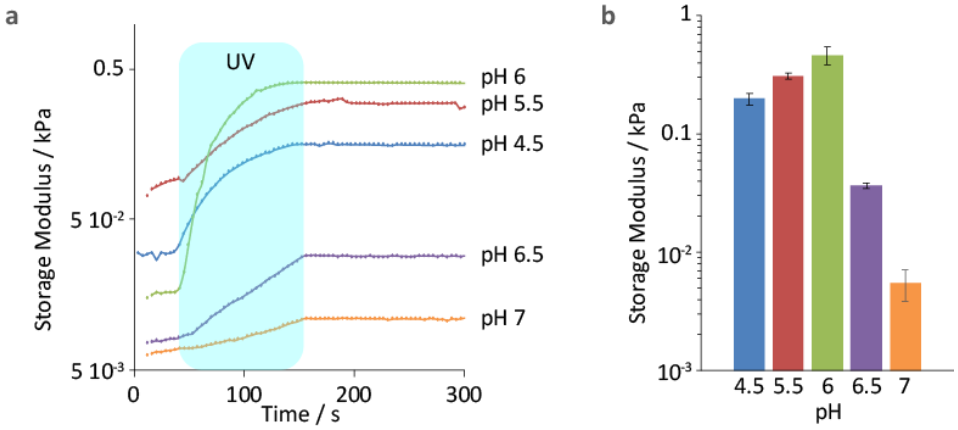

Figure 4. Charcaterisation of the shear mechanical properties of thiol-ene hydrogels based on **P5** (10 mg/mL) and PEGDT, at different pH. a) Evolution of the storage modulus as a function of time and (b) summary of the corresponding storage moduli measured at a frequency of 1 Hz and 1 % strain. The thiol:ene ratio was 1:1 in all cases, the exposure was 120 s at 17 mW/cm^2 UV intensity, starting after 30 s of measurement (blue box). See Table 2 for further details.

Impact of the pH of the medium on UV- and visible light initiated thiol-ene coupling. Having determined how the molecular environment impacts on thiol-ene coupling to a range of polymer backbones, we next investigated how such factors translated into changes in crosslinking and rheological properties of corresponding hydrogels. We first investigated the role of the pH on pentenyl-functionalised carboxymethyl cellulose **P5**, using photo-rheology.

Hydrogel mixtures (100 μL, containing **P5**, the crosslinker poly(ethylene glycol dithiol) (PEGDT) at a 1/2 thiol/alkene) were placed between two methacrylate-functionalised coverslips fixed to the geometries of the rheometer, to ensure chemical coupling and effective stress transmission at the interface[36], followed by irradiation with UV light (360 nm). At pH 6.0, the storage shear modulus rose quickly following the start of photoinitiation and reached a plateau at 500 Pa (for a 10 mg/mL, 1 wt%, gel) within 2 min of irradiation (Figure 4a). Although similar trends were observed at all pH tested, the ultimate modulus reached after 2 min of curing varied significantly with pH (Figures 4 and S14). At pH above 6.0, the modulus of the corresponding gels rapidly decreased below 100 Pa and gels above a pH of 7.4 failed to gel properly, mirroring the sharp decrease in coupling of acetyl cysteine to **P5** at these pH. At lower pH, the storage shear moduli of hydrogels was more stable, although it reduced slightly from 464 ± 80 Pa to 198 ± 22 Pa, perhaps reflecting conformational changes and associated reduction in the hydrodynamic diameter of carboxymethyl cellulose at lower pH. Such changes in the conformation of polymer chains affects molecular diffusion, but could also have an impact on the degree of loop formation (and therefore network defects) resulting from increased intramolecular coupling.

Similarly, the norbornene-functionalised carboxymethyl cellulose and hyaluronic acid **P6** and **P7** displayed similar trends, with maxima in storage shear moduli near neutral pH (Figure 5). However, even at pH 11.0, hydrogels retained moduli above 148 ± 45 Pa and 184 ± 22 Pa (for **P6** and **P7**, respectively), in agreement with the residual coupling efficiency displayed at this pH (Figure 3c), compared to the absence of any reaction in the case of **P5** at the same pH (Figure 2a). The functionalisation levels achieved for **P5**, **P6** and **P7** (13.4, 22.5 and 19.0 %, respectively) correspond to 137, 215 and 91 alkene moieties per polymer chains, respectively. Hence, at neutral pH, with a coupling efficiency of 88 %, **P6** should display 189 crosslinks per chains, on average. At pH 11.0, with a coupling efficiency of 8.9

%, the number of crosslinks is predicted to decrease to 19, a number still sufficient to sustain the formation of a macroscopic gel. In contrast, **P5** should not support the formation of crosslinks at this pH, based on its lack of reactivity with aceyl cysteine. Although reactivity with PEGDT is likely to differe to that of acetyl cysteine, due to reduction in thiol-ene efficiency observed for polymer-polymer coupling[49], reactivity trends observed account for trends in shear mechanical properties of the resulting hydrogels. At lower pH, the shear moduli of the hydrogels generated also decreased (Figure 5a), in line with the observed coupling efficiency measured at pH below 7.0 (Figure 3c). This phenomenon was comparable in the case of **P6** and **P7** to the reduction in modulus observed in the same pH range for **P5**.

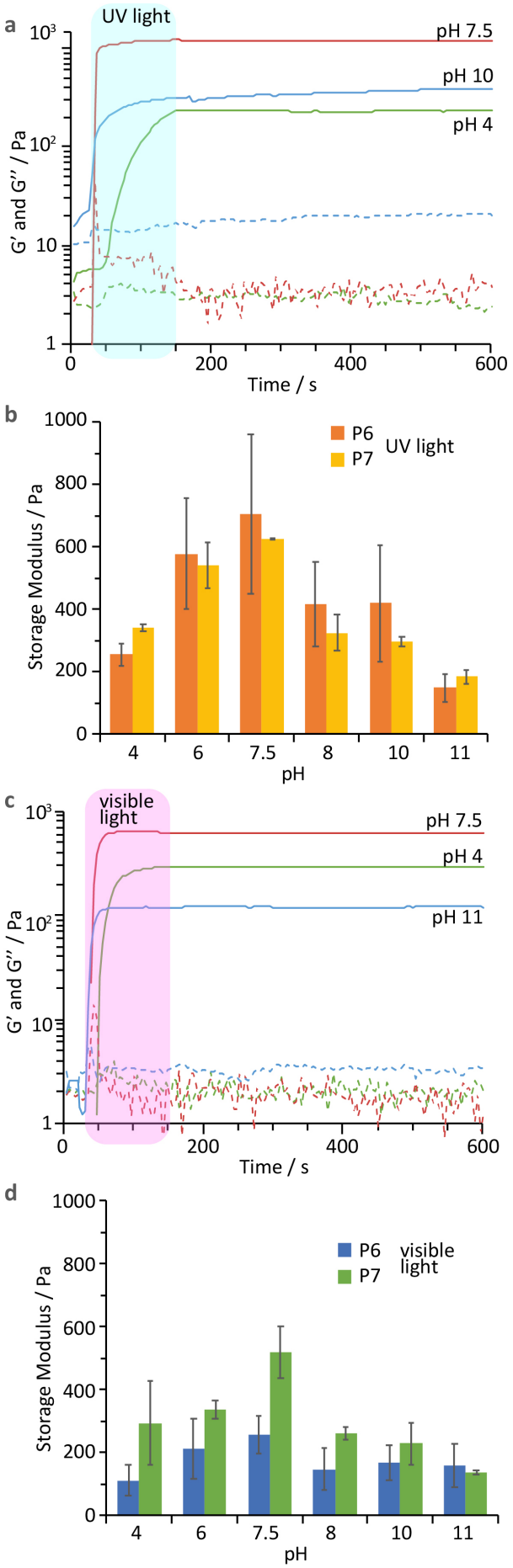

Figure 5. Charcaterisation of the shear mechanical properties of thiol-norbornene hydrogels based on **P6** and **P7** (10 mg/mL) and PEGDT, at different pH. a) Evolution of the storage modulus as a function of time for curing of **P6** with UV light at different pH and (b) summary of storage moduli measured at a frequency of 1 Hz and 1 % strain at a wider range of pH for **P6** and **P7**. The thiol:ene ratio was 1:1 in all cases, the exposure was 120 s at 17 mW/cm^2 UV intensity, starting after 30 s of measurement (blue box). c) Evolution of the storage modulus as a function of time for curing of **P7** with visible light at different pH and (d) summary of storage moduli measured at a frequency of 1 Hz and 1 % strain at a wider range of pH for **P6** and **P7**. The thiol:ene ratio was 1:1 in all cases, the exposure was 120 s at 50 mW/cm^2 visible intensity, starting after 30 s of measurement (purple box). See Tables 2 and 3 for further details.

The crosslinking of **P6** and **P7** with visible light photo-initiation was next explored (Figure 5c and d). We compared these systems at identical polymer concentrations (10 mg/mL, 1 wt%), PEGDT crosslinker concentration (2.33 mg/mL for P6 and 3.45 mg/mL for P7, thiol:alkene 1:1). Similary to the UV-initiated system, with Eosin Y and visible light initiation (400-1300 nm), we observed maximum storage shear moduli at neutral pH (255 $\pm$ 60 and 519 $\pm$ 82 Pa for **P6** and **P7** respectively). These moduli are comparable to those measured with UV-light initiation, in line with the comparable coupling efficiency measured for norbornene carboxylic acid with acetyl cysteine at neutral pH in both initiation conditions (Figure 3a). Similarly to UV-initiated systems, shear moduli decreased at higher and lower pH, although remaining above 100 Pa. This is in agreement with the coupling efficiencies observed on the same pH range. The moduli measured for **P6** were overall lower than those measured for **P7**, perhaps reflecting difference in conformation between these two polymers (and therefore changes in the formation of loops not contributing to networks). All hydrogels displayed frequency sweep and stress relaxation profiles typical of elastomeric networks (Figure S15). Hence, our results indicate that visible light initiation displays a comparable efficiency to UV-initiated systems for norbornene derivatives. However, we point out that visible light initiation failed to promote thiol-ene coupling with non-activated alkenes such as pentenoic acid (with coupling efficiencies below 18 % at all pH tested, using the same quantification protocole used for Figure 3a). Hence, this initiation system is found to be less permissive in terms of molecular structure and pH range, but to display comparable efficiencies at neutral pH with norbornene derivatives.

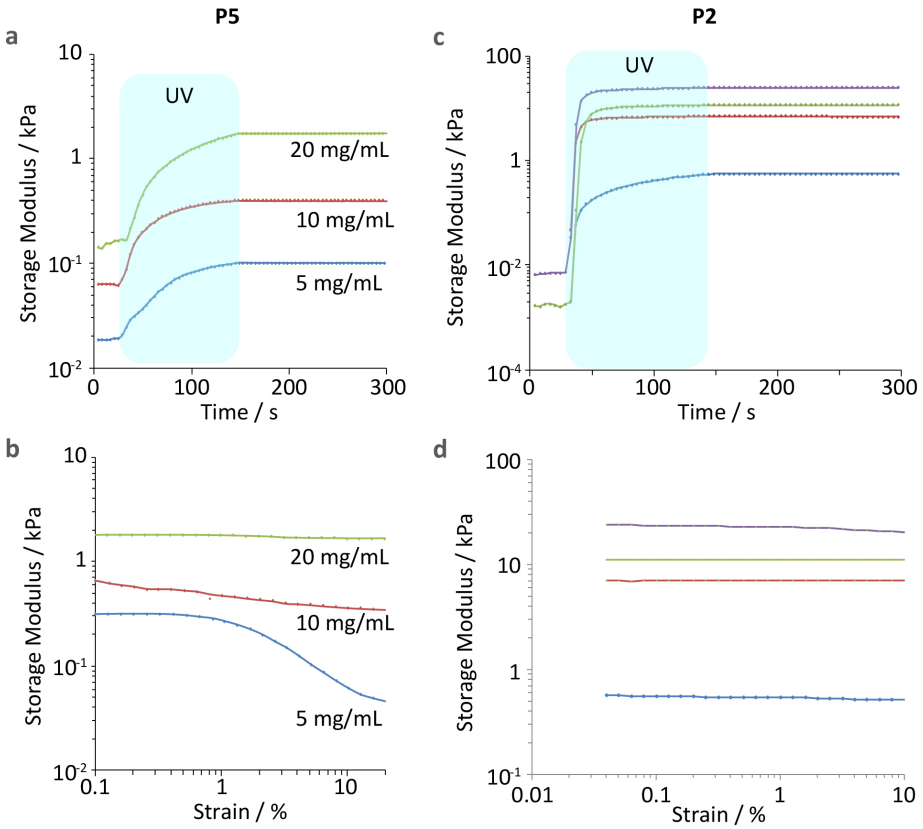

Figure 6. Charcaterisation of the shear mechanical properties of thiol-ene hydrogels based on **P5** and **P2** with PEGDT, at different polymer backbone concentrations. a) **P5** gels at different concentrations. Evolution of the storage modulus as a function of time (frequency of 1 Hz and 1 % strain) and (b) corresponding strain sweeps (frequency of 1 Hz). The alkene/thiol ratio was kept at 1/1 in all cases, the exposure was 120 s at 17 mW/cm^2 UV intensity, starting after 30 s of measurement (blue box). c) Hydrodgels formed from **P2** at different polymer backbone concentrations (blue, S2, 90 mM; red, S3, 135 mM; green, S4, 180 mM; purple, S5, 225 mM; see Table 1 for full details). Evolution of the storage modulus as a function of time (frequency of 1 Hz and 1 % strain). d) Corresponding strain sweeps (frequency of 1 Hz). The alkene/thiol ratio was kept at 2/1 in all cases, the exposure was 120 s at 17 mW/cm^2 UV intensity, starting after 30 s of measurement (blue box). See Tables 1 and 2 for further details.

Impact of the polymer composition and structure on hydrogel mechanics. Given the importance of polymer concentration on hydrogel mechanics, we confirmed that the macromolecule concentration significantly impacted the final moduli of thiol-ene hydrogels (Figure 6). Increasing the concentration of the neutral poly(2-alkyl-2-oxazoline) **P2** from 22.5 to 56.3 mg/mL resulted in an increase in storage shear modulus from 430 Pa to 16.4 kPa (Table 1). Similarly, increasing the concentration of the polyanionic carboxymethyl cellulose **P5** from 5 to 20 mg/mL resulted in an increase in the storage shear modulus from 190 Pa to 1.93 kPa (Table 2). Interestingly, although at an alkene concentration of 9.5 mM **P5** led to a modulus of 1.93 kPa, at a concentration nearly ten times higher (90 mM), **P2** led to a modulus of 430 Pa only. This may be due to some extent to a slight difference in thiol:alkene

ratios (0.64 and 0.5, respectively), but is also a direct reflection of the difference in macromolecular architecture of these two polymers. Hence, despite a molar mass of 1830 g/mol per alkene residue, significantly higher for **P5** than **P2** (686 g/mol, 15 % alkene functionalisation), which should lead to an increase in mesh size, **P5** was significantly stiffer, even at a lower concentration. However, the total number of alkenes per chains of **P5** (137, compared to 9 for **P2**) and the predicted number of crosslinks per chain (62, compared to 8.5 for **P2**) will be higher for the carboxymetyl cellulose based hydrogels. In comparison, at lower concentrations, comparable to those used for **P5**, **P2** and **P3** did not form macroscopic hydrogels. In addition, the more extended conformation expected from the negatively charged **P5** and its higher overall molecular weight will promote the formation of more extended networks with fewer loop defects. Finally, the formation of secondary physical crosslinks, although not contributing significantly to network mechanics individually, may collectively result in a stiffening of associated materials. This is reflected in the increase in viscosity and shear moduli measured prior to crosslinking in the case of **P5** (Figure 6a).

We next examined the impact of the positively charged **P1** and the negatively charged **P3** on the concentration dependent behaviour of corresponding hydrogels (Figure 7). In these cases too, the hydrogel storage shear modulus increased with the polymer concentration. However, at comparable polymer concentrations, the modulus of **P1** and **P3**-based hydrogels was higher than that of **P2** (e.g. 7.5 and 11.1 kPa for 45 and 48 mg/mL **P1** and **P3** gels compared to 430 Pa for **P2** at 60 mg/mL; see Table 1). Hence the concentration of alkene moieties was a better predictor of the modulus of these materials, considering the relatively comparable crosslinking efficiencies measured for these three polymers at neutral pH (Figure 2). Further differences in moduli achieved are likely due to overall polymer concentrations required, differences in molecular weight of the corresponding polymers and their molecular conformation (more elongated for densely charged polymers), as well as repulsions between polymer chains. For example, despite a high number of alkene moieties

per chain for **P1** (300 olefins per macromolecule), and a relatively high molecular weight (68 kDa), it resulted in hydrogels with reduced storage shear moduli at the same alkene concentration.

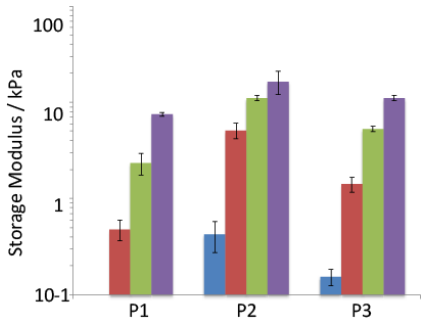

Figure 7. Summary of the storage moduli measured for gels based on backbones **P1-P3**, with different compositions (**S2**, blue; **S3**, red; **S4**, green; S5 purple). The alkene/thiol ratio was kept at 2/1 in all cases, the exposure was 120 s at 17 mW/cm^2 UV intensity, with 5 mol% photoinitiator.

Cell encapsulation within thiol-ene based hydrogels. Having identified some of the factors regulating hydrogel formation via thiol-ene radical coupling, we then explored the use of these materials for cell encapsulation. We first examined the swelling of hydrogels **P1-P5**, quantified via the determination of water contents via TGA (Figure S13 and S16), owing to the importance of changes in water content after cell encapsulation on mechanical properties and cell survival[29]. Swelling levels correlated with the polymer contents introduced during the preparation of the solutions of precursors prior to gelation (Tables 1 and 2). Hence the relatively low polymer densities associated with **P5** hydrogels studied led to very limited swelling levels (Figure S16). In addition, swellings were found to be more pronounced in deionised water, in agreement with the associated increased osmotic pressure. Overall, the swelling levels measured for **P1-P5** remained below 20% and were considered reasonable for cell encapsulation.

To investigate eventual cytotoxic effects induced during encapsulation, human umbilical vein endothelial cells (HUVECs) were seeded in hydrogels generated from **P1-P5** (Figure 8). As these gels were designed to display an excess of alkenes, we were able to introduce

additional cysteine-bearing RGD peptides to promote cell adhesion. Viability levels were compared to those of cells cultured on 2D tissue culture plastic (Ctrl.). Cells encapsulated in hydrogels based on the polycationic **P1** died rapidly, due to its strong electrostatic charge density able to disrupt cell membranes. However, most cells seeded in the other hydrogels appeared to survive after 24 h of culture. We note that even cells seeded in **P5**, which was formed at a slightly lower pH (pH 6.0) to promote efficient network formation (prior to exchanging with medium shortly after curing of these hydrogels) remained viable. However, cells loaded in **P4**-based hydrogels displayed reduced viability levels, perhaps owing to the high charge density associated with this material and its stronger swelling, even in PBS (Figure S16). Considering the lack of cell-mediated degradability of these hydrogels, the lack of cell spreading was unsurprising.

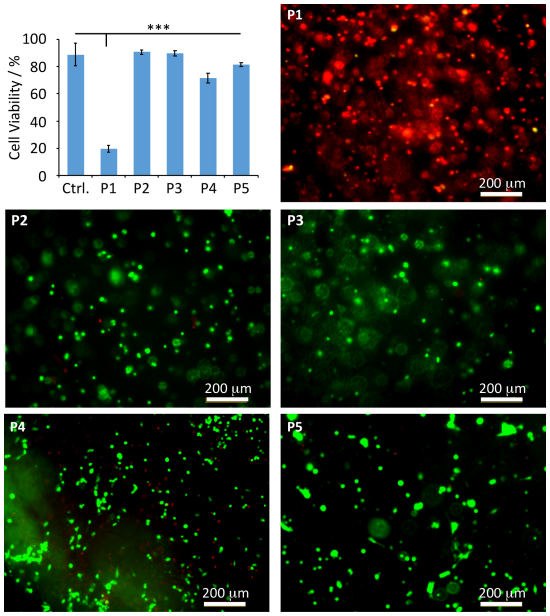

Figure 8. Viability of HUVECs encapsulated in non-degradable PEGDT crosslinked hydrogels with backbones **P1-P5** after 24h of culture (cell densities of 1 million cells/mL) and corresponding fluorescence microscopy images. Live cells were stained green and dead cells red. Gels P1-P3 were generated with alkene/thiol ratios of 2:1, 10 mol% RGD, 5 mol% photoinitiator and 120 s UV exposure. **P4** and **P5** were made with alkene ratio of 2:1, 10 mol% RGD, 5 mol% photoinitiator and 120s UV. Gels were made at the pH relevant to biological conditions and showing good conversion levels (Figure 2): **P1**, pH 7.4; **P2**, pH 7.4; **P3**, pH 7.4; **P4**, pH 7 and **P5**, pH 6.

We next examined the impact of hydrogel mechanics on cell viability, focusing on the poly(ethylene glycol) analogue **P2**-based system. HUVECs were seeded in hydrogels displaying shear storage moduli ranging from 430 Pa to 16.4 kPa (see Table 1, entries $P2_{S2}$-$P2_{S5}$) and cultured for 24 h. Although cells remained rounded in these hydrogels (all were crosslinked with the non-degradable PEGDT) viabilities were high at all stiffnesses (Figure S17). To confirm the generality of these results, we investigated the viability of dermal fibroblasts in poly(2-ethyl-2-oxazoline) hydrogels with stiffnesses ranging from 5.1 to 16.4 kPa and observed again high viabilities in all conditions (Figure S18). When the degradability of these networks was increased by replacing PEGDT with a di-cystein peptide bearing the enzymatically cleavable VPM sequence, high viabilities were retained (Figure S18c). Therefore, our results demonstrate the potential of poly(2-oxazoline) based hydrogels to safely encapsulate cells in matrices with controlled mechanics and degradation.

Conclusions

Thiol-ene based hydrogels are particularly attractive for cell encapsulation as the mild character of this crosslinking chemistry has minor impact on cell viability and can be triggered with UV as well as visible light. Our work indicates the importance of the molecular microenvironment on the efficiency of radical thiol-ene coupling. However, we find that thiol-ene efficiencies remain high at neutral pH for most polymer architectures tested, except those displaying particularly high negative charge densities. This was proposed to be due to changes in thiol densities and local diffusion, limiting coupling, although deprotonation of thiols by basic residues of the polymer backbone cannot be excluded. Therefore, the impact of peptide chemistry on such diffusion and associated polymer coupling and crosslinking should be investigated more systematically, to fully determine the freedom with which peptide sequences can be engineered independently of thiol-ene radical coupling. We also found that thiol-ene efficiencies in visible light-initiated systems remain high on a sufficiently broad pH range centered around neutral pH, providing that activated norbornene moieties are used, with minimal impact on the mechanics of the resulting matrices. The non-activated olefins tested were found to display very limited reactivity using this initiating system. Visible light initiation remains incompatible with classic fully supplemented cell culture media though and requires the use of media unsupplemented with phenol red, or PBS, at least for curing. Beyond a more thorough investigation of the impact of peptide sequence on polymer coupling and hydrogel crosslinking, the impact of molecular structure on the coupling of other macromolecules, mimicking other properties of the extra-cellular matrix or conferring additional properties such as drug delivery or nanoparticle coupling should be characterised systematically.

Supporting information

The Supporting Information is available free of charge at https://pubs.acs.org/doi/. Additional NMR, FTIR, GPC, TGA, rheology and cell viability characterisation.

Author Information

Corresponding Author.

*E-mail: j.gautrot@qmul.ac.uk.

Notes.

The authors declare no competing financial interest.

Acknowledgment

B.C. thanks Queen Mary, University of London for her PhD studentship. L.W. thanks the Chinese Scholarship Council (grant no 201506550007). This work was supported by European Research Council (ProLiCell, 772462).

References

1. Caliari, S. R.; Burdick, J. A., A practical guide to hydrogels for cell culture. *Nat. Methods* **2016,** *13* (5), 405-414.
2. Xu, Z.; Bratlie, K. M., Click chemistry and material selection for *in situ* fabrication of hydrogels in tissue engineering applications. *ACS Biomater. Sci. Eng.* **2018,** *4*, 2276-2291.
3. Kharkar, P. M.; Rehman, M. S.; Skeens, K. M.; Maverakis, E.; Kloxin, A. M., Thiol-ene click hydrogels for therapeutic delivery. *ACS Biomater. Sci. Eng.* **2016,** *2* (2), 165-179.
4. Jiang, Y.; Chen, J.; Deng, C.; Suuronen, E. J.; Zhong, Z., Click hydrogels, microgels and nanogels: Emerging platforms for drug delivery and tissue engineering. *Biomaterials* **2014,** *35*, 4969-4985.
5. Colak, B.; di Cio, S.; Gautrot, J. E., Biofunctionalised patterned polymer brushes via thiol-ene coupling for the control of cell adhesion and the formation of cell arrays. *Biomacromolecules* **2018,** *19* (5), 1445-1455.
6. Tan, K. Y.; Ramstedt, M.; Colak, B.; Huck, W. T. S.; Gautrot, J. E., Study of thiol-ene chemistry on polymer brushes and application to surface patterning and protein adsorption *Polym. Chem.* **2016,** *7*, 979-990.
7. Ahmad, N.; Colak, B.; Gibbs, M. J.; Zhang, D. W.; Gautrot, J. E.; Watkinson, M.; Becer, C. R.; Krause, S., Peptide cross-linked poly(2-oxazoline) as a sensor material for the detection of proteases with a quartz crystal microbalance. *Biomacromolecules* **2019,** *7*, 2506-2514.
8. Ahmad, N.; Colak, B.; Zhang, D. W.; Gibbs, M. J.; Watkinson, M.; Becer, C. R.; Gautrot, J. E.; Krause, S., Peptide cross-linked poly(ethylene glycol) hydrogel films as biosensor coatings for the detection of collagenase. *Sensors* **2019,** *19*, 1677.
9. Gould, S. T.; Darling, N. J.; Anseth, K. S., Small peptide functionalized thiol-ene hydrogels as culture substrates for understanding valvular interstitial cell activation and *de novo* tissue deposition. *Acta Biomater* **2012,** *8*, 3201-3209.
10. Neumann, A. J.; Quinn, T.; Bryant, S. J., Nondestructive evaluation of a new hydrolytically degradable and photo-clickable PEG hydrogel for cartilage tissue engineering. *Acta. Biomaterialia* **2016,** *39*, 1-11.
11. Wade, R. J.; Bassin, E. J.; Gramlich, W. M.; Burdick, J. A., Nanofi brous Hydrogels with Spatially Patterned Biochemical Signals to Control Cell Behavior. *Adv. Mater.* **2015,** *27* (8), 1356-1362.
12. Cai, S.; Liu, Y.; Shu, X. Z.; Prestwich, G. D., Injectable glycosaminoglycan hydrogels for controlled release of human basic fibroblast growth factor. *Biomaterials* **2005,** *26*, 6054-6067.
13. Fu, Y.; Xu, K.; Zheng, X.; Giacomin, A. J.; Mix, A. W.; Kao, W. J., 3D cell entrapment in crosslinked thiolated gelatin-poly(ethylene glycol) diacrylate hydrogels. *Biomaterials* **2012,** *33*, 48-58.
14. Gramlich, W. M.; Kim, I. L.; Burdick, J. A., Synthesis and orthogonal photopatterning of hyaluronic acid hydrogels with thiol-norbornene chemistry. *Biomaterials* **2013,** *34*, 9803-9811.
15. Khetan, S.; Guvendiren, M.; Legant, W. R.; Cohen, D. M.; Chen, C. S.; Burdick, J. A., Degradation-mediated cellular traction directs stem cell fate in covalently crosslinked three-dimensional hydrogels. *Nat. Mater.* **2013,** *12*, 458-465.
16. Trappmann, B.; Baker, B. M.; Polacheck, W. J.; Choi, C. K.; Burdick, J. A.; Chen, C. S., Matrix degradability controls multicellularity of 3D cell migration. *Nat. Commun.* **2017,** *8*, 371.
17. Ruskowitz, E. R.; DeForest, C. A., Proteome-wide Analysis of Cellular Response to Ultraviolet Light for Biomaterial Synthesis and Modification. *ACS Biomater. Sci. Eng.* **2019,** *5* (5), 2111-2116.

18. Costa, P.; Gautrot, J. E.; Connelly, J., Directing cell migration using micropatterned and dynamically adhesive polymer brushes. *Acta Biomater* **2014,** *10* (6), 2415-2422.
19. Marklein, R. A.; Burdick, J. A., Spatially controlled hydrogell mechanics to modulate stem cell interactions. *Soft Matter* **2010,** *6*, 136-143.
20. Cramer, N. B.; Bowman, C. N., Kinetics of thiol-ene and thiol-acrylate photopolymerizations with real-time fourier transform infrared. *J. Polym. Sci., A: Polym. Chem.* **2001,** *39*, 3311-3319.
21. Cramer, N. B.; Reddy, S. K.; O'Brien, A. K.; Bowman, C. N., Thiol-ene photopolymerization mechanism and rate limiting step changes for various vinyl functional group chemistries. *Macromolecules* **2003,** *36* (21), 7964-7969.
22. Reddy, S. K.; Cramer, N. B.; Bowman, C. N., Thiol-vinyl mechanisms. 1. Termination and propagation kinetics in thiol-ene pohotpolymerizations. *Macromolecules* **2006,** *39*, 3673-3680.
23. Northrop, B. H.; Coffey, R. N., Thiol-ene click chemistry: computational and kinetic analysis of the influence of alkene functionality. *J. Am. Chem. Soc.* **2012,** *134*, 13804-13817.
24. Colak, B.; Da Silva, J. C. S.; Soares, T. A.; Gautrot, J. E., Impact of the molecular environment on thiol-ene coupling for biofunctionalization and conjugation. *Bioconj. Chem.* **2016,** *27* (9), 2111-2123.
25. Fu, A.; Gwon, K.; Kim, M.; Tae, G.; Kornfield, J. A., Visible-light-initiated thiol-acrylate photopolymerization of heparin-based hydrogels. *Biomacromolecules* **2015,** *16*, 497-506.
26. Lin, T.-Y.; Bragg, J. C.; Lin, C.-C., Designing Visible Light-Cured Thiol-Acrylate Hydrogels for Studying the HIPPO Pathway Activation in Hepatocellular Carcinoma Cells. *Macromol. Biosci.* **2016,** *16*, 496-507.
27. Hao, Y.; Lin, C.-C., Degradable thiol-acrylate hydrogels as tunable matrices for three-dimensional hepatic culture. *J. Biomed. Mat. Res. A* **2014,** *102A* (11), 3813-3827.
28. Hao, Y.; Shih, H.; Munoz, Z.; Kemp, A.; Lin, C.-C., Visible light cured thiol-vinyl hydrogels with tunable degradation for 3D cell culture. *Acta Biomater* **2014,** *10*, 104-114.
29. Young, S. A.; Riahinezhad, H.; Amsden, B. G., In situ-forming, mechanically resilient hydrogels for cell delivery. *J. Mat. Chem. B* **2019,** *7*, 5742-5761.
30. Greene, T.; Lin, T.-Y.; Andrisani, O. M.; Lin, C.-C., Comparative study of visible light polymerized gelatin hydrogels for 3D culture of hepatic progenitor cells. *J. Appl. Polym. Sci.* **2017,** *134*, 44585.
31. Baudis, S.; Bomze, D.; Markovic, M.; Gruber, P.; Ovsianikov, A.; Liska, R., Modular Material System for the Microfabrication of Biocompatible Hydrogels Based on Thiol–Ene-Modified Poly(vinyl alcohol). *J. Polym. Sci., A: Polym. Chem.* **2016,** *54*, 2060-2070.
32. Miquelard-Garnier, G.; Demoures, S.; Creton, C.; Hourdet, D., Synthesis and Rheological Behavior of New Hydrophobically Modified Hydrogels with Tunable Properties. *Macromolecules* **2006,** *39*, 8128-8139.
33. Grube, S.; Oppermann, W., Inhomogeneity in hydrogels synthesized by thiol-ene polymerization. *Macromolecules* **2013,** *46*, 1948-1955.
34. Li, Y.; Tan, Y.; Xu, K.; Lu, C.; Wang, P., A biodegradable starch hydrogel synthesized via thiol-ene click

chemistry. *Polym. Degrad. Stab.* **2017,** *137*, 75-82.
35. Shih, H.; Lin, C.-C., Cross-Linking and Degradation of Step-Growth Hydrogels Formed by Thiol−Ene Photoclick Chemistry. *Biomacromolecules* **2012,** *13*, 2003-2012.
36. Megone, W.; Roohpour, N.; Gautrot, J. E., Impact of surface adhesion and sample heterogeneity on the multiscale mechanical charcaterisation of soft biomaterials. *Sci. Rep.* **2018,** *8*, 6780.

37. Colak, B., Peptide Based Biomaterials via Thiol-ene Chemistry. *Queen Mary, University of London* **2016**.
38. Mathew, A.; Cao, H.; Collin, E.; Wang, W.; Pandit, A., Hyperbranched PEGmethacrylate linear pDMAEMA block copolymer as an efficient non-viral gene delivery vector. *International Journal of Pharmaceutics* **2012,** *434* (1-2), 99-105.
39. Gress, A.; Volkel, A.; Schlaad, H., Thio-click modification of poly 2-(3-butenyl)-2-oxazoline. *Macromolecules* **2007,** *40* (22), 7928-7933.
40. Schenk, V.; Ellmaier, L.; Rossegger, E.; Edler, M.; Griesser, T.; Weidinger, G.; Wiesbrock, F., Water-Developable Poly(2-oxazoline)-Based Negative Photoresists. *Macromolecular Rapid Communications* **2012,** *33* (5), 396-400.
41. Dadoo, N.; Landry, S. B.; Bomar, J. D.; Gramlich, W. M., Synthesis and Spatiotemporal Modification of Biocompatible and Stimuli-Responsive Carboxymethyl Cellulose Hydrogels Using Thiol-Norbornene Chemistry. *Macromol. Biosci.* **2017,** *17*, 1700107.
42. Stephens, P.; Grenard, P.; Aeschilmann, P.; Langley, M.; Blain, E.; Errington, R.; Kipling, D.; Thomas, D.; Aeschlimann, D., Crosslinking and G-protein functions of transglutaminase 2 contribute differentially to fibroblast wound healing responses. *Journal of Cell Science* **2004,** *117* (15), 3389-3403.
43. Hoyle, C. E.; Bowman, C. N., Thiol-ene click chemistry. *Angew. Chem., Int. Ed.* **2010,** *49*, 1540-1573.
44. Serjeant, E. P.; Dempsey, B., *Ionization constants of organic acids in aqueous solutions*. Pergamon Press: Oxford, 1979.
45. Murmiliuk, A.; Košovan, P.; Janata, M.; Procházka, K.; Uhlík, F.; Štěpánek, M., Local pH and Effective pK of a Polyelectrolyte Chain: Two Names for

One Quantity. *ACS Macro Lett.* **2018,** *7*, 1243-1247.
46. Nova, L.; Uhlı, F.; Kosovan, P., Local pH and effective pKA of weak polyelectrolytes – insights from computer simulations. *Phys. Chem. Chem. Phys.* **2017,** *19*, 14376-14387.
47. Lin, C.-C.; Raza, A.; Shih, H., PEG hydrogels formed by thiol-ene photo-click chemistry and their effect on the formation and recovery of insulin-secreting cell spheroids. *Biomaterials* **2011,** *32*, 9685-9695.
48. Fairbanks, B. D.; Schwartz, M. P.; Halevi, A. E.; Nuttelman, C. R.; Bowman, C. N.; Anseth, K. S., A versatile synthetic extracellular matrix mimic via thiol-norbornene photopolymerization. *Adv. Mater.* **2009,** *21*, 5005-5010.
49. Koo, S. P. S.; Stamenovic, M. M.; Prasath, R. A.; Inglis, A. J.; Du Prez, F. E.; Barner-Kowollik, C.; Van Camp, W.; Junkers, T., Limitations of radical thiol-ene reactions for polymer-polymer conjugation. *J. Polym. Sci., A: Polym. Chem.* **2010,** *48* (8), 1699-1713.